Cryosphere Models: Ocean and Land

in the ENCYCLOPEDIA OF SUSTAINABILITY SCIENCE AND TECHNOLOGY

section on *Climate Change Modeling and Methodology*

by Cecilia M. Bitz[1] and Shawn J. Marshall[2]

[1] Atmospheric Sciences Department, University of Washington, Atmospheric Sciences box 351640, Seattle WA 98195-1640, USA. Tel: 206-543-1339; bitz@atmos.washington.edu
[2] Department of Geography, University of Calgary, Earth Sciences 356, 2500 University Dr NW, Calgary AB T2N 1N4, Canada. Tel: 403-220-4884; shawn.marshall@ucalgary.ca

Abstract

The global cryosphere encompasses snow and ice in all its forms in the natural environment, including glaciers and ice sheets, sea ice, lake and river ice, permafrost, seasonal snow, and ice crystals in the atmosphere. Cryospheric models are mathematical and numerical descriptions of these components of the Earth system, designed to simulate snow and ice processes and feedbacks in the context of the global climate system. This entry covers all forms of ice except ice crystals in the atmosphere, which are more appropriately combined with clouds and appear in encyclopedia entry "Cloud Albedo Enhancement for Solar Radiation Management" and "Cloud System Models". We focus on models that are appropriate for global climate modeling. There are regional climate modeling applications that include some of the cryospheric components discussed here as well.

Article Outline
Glossary
Definition of the Subject
Introduction
Several full numbered sections
Future Directions
Bibliography

Glossary

Ablation. Snow and ice removed from an ice mass via meltwater runoff, sublimation, wind scour, or glacial calving (mechanical fracturing and separation).

Accretion. Increase in ice mass by basal growth in the case of floating ice, the compression of snow into ice, or freezing of water that has pooled on the ice or percolated into snow from rain, meltwater, or flooding of sea/lake/river water.

Accumulation. Snow and ice added to an ice mass via snowfall, frost deposition, rainfall that freezes on/in the ice mass, refrozen meltwater, wind-blown snow deposition, and avalanching.

Mass Balance. The overall gain or loss of mass for a component of the cryosphere over a specified time interval, typically one year. This can be expressed as a rate of change of mass (kg yr^{-1}), ice volume (m^3 yr^{-1}), or water-equivalent volume (m^3 w.eq. yr^{-1}). It is also common to express this as the area-averaged rate of change or the specific mass balance rate, with units of kg m^{-2} yr^{-1} or m w.eq. yr^{-1}.

Glacier. A perennial terrestrial ice mass that shows evidence of motion/deformation under gravity.

Grounding Line. The transition zone between grounded and floating ice.

Ice Sheet. A large (i.e., continental-scale) dome of glacier ice that overwhelms the local bedrock topography, with the ice flow direction governed by the shape of the ice cap itself.

Icefield. A sheet of glacier ice in an alpine environment in which the ice is not thick enough to overwhelm the local bedrock topography, but is draped over and around it; glacier flow directions in an icefield are dictated by the bed topography.

Ice Shelf. Glacier ice that has flowed into an ocean or lake and is floating, no longer supported by the bed.

Lake/River Ice. Floating ice on rivers or lakes, usually freshwater ice.

Permafrost. Perennially frozen ground, technically defined as ground that is at or below 0°C for at least two years.

Soil Ice. Ice in permafrost.

Sea Ice. Floating ice from frozen seawater.

Snow. Ice-crystal precipitation that accumulates on the surface.

1 Definition of Subject

The global cryosphere encompasses snow and ice in all its forms in the natural environment, including glaciers and ice sheets, sea ice, lake and river ice, permafrost, seasonal snow, and ice crystals in the atmosphere. Cryospheric models are mathematical and numerical descriptions of these components of the Earth system, designed to simulate snow and ice processes and feedbacks in the context of the global climate system. This entry covers all forms of ice except ice crystals in the atmosphere, which are more appropriately combined with clouds and appear in encylopedia entries "Cloud Albedo Enhancement for Solar Radiation Management" and "Cloud System Modeling".

The cryosphere is critical to understanding global climate change owing to its control on Earth's surface reflectivity. In addition, storage of freshwater by the cryosphere and exchange of freshwater between the cryosphere and ocean are fundamental to ocean circulation and sea level rise. Sea ice and snow insulate the underlying surface and usually allow lower atmospheric temperatures than snow and ice environments. Biogeochemical cycles in sea ice and permafrost influence carbon dioxide and methane concentrations in the atmosphere, and sea ice hosts organisms and nutrients important to marine ecosystems. Modeling cryosphere-climate interactions generally requires modeling the mass balance of ice on Earth and the key features of ice that interact with the climate system.

Perennial ice covers 10.8% of Earth's land, with most of this ice area in the great polar ice sheets in Greenland and Antarctica. Smaller glaciers and icefields are numerous — the global population is estimated at 160,000 — but these ice masses cover less than 1% of the landscape. An additional 15.4% of Earth's land surface is covered by permafrost: frozen ground that ranges from a few meters to 100s of metres deep.

In contrast to this permanent land ice, seasonal snow and ice fluctuate dramatically. Snow cover is the largest-varying element of the cryosphere, with complete summer loss of this snow everywhere on Earth except over Antarctica, the interior of Greenland, and in the accumulation areas of other high-altitude and polar ice caps. In winter, the northern hemisphere snow cover reaches an average maximum extent of 45.2×10^6 km [1], based on data from 1966-2004). This amounts to 49% of the Northern Hemisphere land mass. Because the southern hemisphere continents are situated at lower latitudes (excepting Antarctica), southern snow cover is less extensive, with the seasonal snow cover estimated at 1.2×10^6 km. This combines with the permanent blanket of snow over Antarctica to give a peak southern hemisphere terrestrial snow cover of 15.0×10^6 km.

Relative to the snowpack, seasonal sea ice cycles are more hemispherically symmetric, although there are interesting north-south contrasts. Based on passive microwave remote sensing for the period 1979-2010, the average minimum Northern Hemisphere sea ice area is 4.4×10^6 km, typically reached in September [2]. Maximum ice cover is usually attained in March, with an average area of $13.1 \times 10^6$10km. The annual average Northern Hemisphere sea-ice area is 9.4×10^6 km. The Southern Hemisphere sea ice has a larger seasonal cycle, with relatively little multiyear ice. Annual mean sea ice cover in the south is 8.7×10^6 km, varying from 1.9×10^6 km (February) to 14.5×10^6 km (September).

2   Introduction

The early energy-balance modelers of the 1960s who investigated global climate recognized the importance of the high albedo of ice in the climate system [3, 4]. Their models parameterized snow and ice albedo by varying the land or ocean surface albedo with surface temperature, but no other physical characteristics of ice, such as its ability to insulate or store energy and freshwater, was simulated. When subject to climate forcing, such as a perturbation to the solar constants, the models nonetheless exhibited an amplification of temperature change in the high latitudes — a phenomena widely known as polar amplification. The albedo difference between ice-covered and ice-free regions determined the strength

of the polar amplification. Today we know ice-albedo feedback is only one of many important ways that ice and snow contribute to the climate system.

The next progression in ice modeling among global climate models was to include the major elements of the mass balance of snow on land [5] and sea ice [6], both implemented in the Geophysical Fluid Dynamics Laboratory (GFDL) in 1969. Yet the GFDL model and all other climate model for several more decades had no ice dynamics, continued to treat ice sheets as shallow snow fields with prescribed representative topography, and ignored soil ice altogether. The more advanced aspects of cryosphere modeling evolved in parallel with, but independent of global climate models.

In the 1950s, John Nye [7, 8] laid the theoretical foundations for glacier models, through the elucidation of the essential physics as well as several well-judged simplifications that permit analytical solutions. Theoretical and laboratory analyses by a contemporary materials scientist, John Glen, led to the understanding that glacier ice deforms as a nonlinear viscous fluid. Glen established a constitutive relation for the rheology of glacier ice that endures to this day [9, 10]. Combined with the conservation equations for mass, momentum, and energy, this provides the basis for modeling glaciers and ice sheets. By the late 1960s and 1970s, emerging computer power presented the opportunity to develop numerical models of glaciers [11, 12, 13]. Model development through the 1980s largely focused on regional simulations [14] and ice flow in different regimes, such as ice shelves and ice streams [15, 16].

In the late 1980s Philippe Huybrechts developed the first pragmatic, operational 3D thermomechanical ice sheet model [17, 18]. This model has been applied extensively to the Greenland and Antarctic Ice Sheets, helping to understand their past and present evolution e.g., [19, 20, 21, 22]. The Huybrechts model also underpins the projections of ice sheet response to climate change in the IPCC reports. Similar models have now been developed in several research groups, and intercomparison exercises have been carried out to evaluate model strengths and weaknesses [23, 24].

A few global climate models have incorporated a Huybrechts-type ice sheet model such that changes to the global climate can interact with the shape and extent of ice sheets in Greenland and Antarctica. The interaction occurs through changes in surface albedo as the ice sheet retreats or advances over bare soil, elevation-temperature feedbacks, and through changes in the atmospheric and oceanic circulation [21, 25, 26, 27].

The low-order glacier models implemented in global climate models to date are based on a simplified representation for ice sheet flow (see section 4), which is not well-suited to ice shelves, ice streams, and ice sheet margins. Because these features of ice sheets are known to be changing rapidly, current development efforts are focusing on higher-order solutions of ice dynamics [28, 29, 30, 31, 32]. Models of valley glacier dynamics have followed a similar evolution from simplified representations of ice dynamics, e.g.[33], to recent simulations that include a more complete representation of the glacier stress and strain regime [34, 35, 36, 37, 38]. Parallel to this recent effort are formal, community-scale programs to couple more sophisticated, high-resolution ice sheet models into global climate models [39], although fully-coupled efforts with global climate models are still in their infancy.

The development of sea ice models took a rather different path than glacial models. Model development began later, but the methods, albeit often simplified, migrated more quickly

into global climate models. Today the lag between developing new sea ice model physics and implementing them in global climate models is often only a few years.

The first sea ice rheology was proposed in the 1970s, roughly two decades after the glacier rheology proposed by Nye and Glen. Initially a plastic rheology was put forward as a way to produce deformation (ridging and rafting) for the Arctic Ice Dynamics Joint Experiment (AIDJEX) model spearheaded by Max Coon [40]. Models attempting to treat ice as a plastic were only appropriate for local-scale problems of a few weeks to a month duration and could not be used to investigate ice-climate interactions owing to their inherent numerical complexity [41]. In the late 1970s, William Hibler proposed a nonlinear viscous plastic (VP) rheology — a simplification motivated on physical grounds [42]. In a 1979 landmark paper, Hibler applied his sea ice model to the whole Arctic Ocean basin and ran an 8-year simulation [43]. The AIDJEX and Hibler sea ice dynamics remains the foundation of modern sea ice models.

A sub-grid scale parameterization of the variety of sea ice thicknesses that are found in a typical model grid box, known as an ice-thickness distribution (ITD), was developed by Alan Thorndike and colleagues [44] and implemented by Hibler at the basin-scale in 1980 [43]. Modeling the intricacies of sea ice thermodynamics to account for the thermal inertia of brine-pocket physics was developed slightly earlier by Norbert Untersteiner and Gary Maykut [45, 46], but it was only implemented in 1D until the present decade.

The first global climate models treated sea ice as a uniform slab without leads (openings among floes), melt ponds, or brine pockets, based on the simplifications proposed by Albert Semtner [47]. If the sea ice moved at all, it was advected with the surface currents — in what is known as "free drift". Once the sea ice thickness reached some threshold (4 m was common) it was then held motionless to prevent the sea ice from building to excess in regions of convergence [48, 49, 50].

It wasn't until Flato and Hibler [51] simplified the VP model by treating sea ice as a cavitating fluid (CF) that global climate modelers attempted to implement sea ice dynamics with a constitutive law. However, the lack of shear strength in the CF model degraded the accuracy of the simulation compared to the VP model. Soon after Hunke and Ducowicz [52] developed a technique of treating sea ice as an elastic-viscous-plastic (EVP) material — a numerical approximation to the VP model that asymptotes to the full VP solution and yet is efficient, highly parallelizable, and offers flexible grid choices. Zhang and Hibler [53] followed suit by making the VP numerics more efficient and parallelizable. These new dynamical schemes ushered in a time of rapid improvement in the sea ice dynamics in climate models, and now EVP and VP dynamics are in wide use among climate models. Thermodynamic advances in global climate models has been slower. The use of an ITD and brine-pocket physics has only been recent in climate models [54, 55]. Melt pond parameterizations and radiative transfer that includes scattering have only been developed in one dimension and are in the early stages of production runs in the next generation of models.

Snow and permafrost models used for one and two-dimensional applications also progressed significantly before their developments were brought into climate models, e.g., [56, 57, 58]. Permafrost models are typically based on one-dimensional thermal diffusion in the upper 2 km of the Earth surface, consisting of bedrock, sediments, and soils. Where temperatures are below freezing, ground ice occupies pore space and fractures in the rock. A freezing front

propagates to a depth that is limited by the geothermal heat flux. Permafrost models simulate the aggradation or degradation of permafrost, based on mean annual surface (ground) temperatures and subject to geothermal heat flux from below. Detailed near-surface models can be added to simulate the seasonal melting/freezing of the surface active layer. In reality more complex thermodynamic and hydrological processes are involved in permafrost dynamics. For instance, water flow can advect heat and there are 3D thermal effects associated with horizontal gradients in surface temperature, arising from variable surface vegetation, micro-topography, snow cover, and surface lakes. In addition, freezing of subsurface water is not always limited to the pore space; ice can accrue as "massive ice" deposits (e.g., ice lenses) through migration of water to the interstices of soils and sediments, driven by low capillary pressures. Simple permafrost models, as used in climate models, typically neglect these processes and focus on large-scale predictions of permafrost depth and 1D ground temperature structure.

For snow models the chief physical processes that prove challenging to model are snow aging and grain size evolution influences on the albedo and density; liquid water infiltration and storage; snow blowing, redistribution, and collection by vegetation; and active layer depth dynamics. Many global climate models have developed terrestrial snow schemes to treat all but snow redistribution in the last few decades because these processes have a major impact on surface albedo, surface hydrology, and soil carbon storage [59, 60, 61, 62, 63, 64]. Sub-gridscale snow distribution models exist [65] but have yet to be implemented in any global climate model that we are aware of. Models of snow on sea ice tend to be more primitive because transporting every variable that describes the snow is necessary and expensive.

In subsequent sections we describe the equations and methods used to model the cryosphere, followed by a brief outlook of future directions and priorities in cryospheric modeling. Components of the cryosphere are grouped into four types based on common characteristics and physics: Land ice refers to ice above the soil/bedrock (e.g., glaciers and ice sheets) and ice shelves; floating ice refers to river, lake, or sea ice; frozen soil includes permafrost and seasonally frozen soil; and finally snow, which may overly land ice, floating ice, or soil. The underlying equations for the dynamics of land and floating ice are rooted in a blend of continuum mechanics and fluid dynamics, but there are significant differences in their implementation, justifying separate descriptions. In contrast, thermodynamics cuts across all aspects of the cryosphere, and much about it can be described more generally.

3 Thermodynamics of the Cryosphere

Conservation of energy

The governing equation for the thermodynamics of the cryosphere is conservation of energy:

$$\frac{Dq}{Dt} + \nabla \cdot (\mathbf{u}_\nu \phi q_\nu) = -\nabla \cdot (k \nabla T) + Q_{sw} + \Phi \tag{1}$$

which is written in terms of an enthalpy (q) for ice, snow, or mixed soil and ice, where q is expressed in units of $\mathrm{J\,m^{-3}}$, ϕ is the void (or pore) fraction within the solid where liquid water/vapor may exist, $\mathbf{u}_\nu$ is the velocity of liquid water/vapor moving in the voids, T is

6

temperature in the solid and voids, q_ν is the enthalpy of liquid water/vapor in the voids, k is the conductivity in solids and voids, Q_{sw} is the absorption of shortwave radiation over a finite thickness of the ice ($\mathrm{W\,m^{-3}}$), which is assumed to be significant only in ice, and Φ is the strain heat production due to deformation work (significant for glaciers). The first term is a Lagrangian derivative of the heat required to raise the temperature and change the phase between solid and liquid. It is Lagrangian to account for the horizontal advection of heat in moving land and floating ice (see sections 4 and 5). The second term represents heat transport due to liquid water or vapor transport in the voids, and the third term is diffusion of heat in both solid and voids. In models of practical use today, vertical gradients in the enthalpy are far greater than those in the horizontal, therefore the horizontal diffusion and horizontal liquid/vapor transport in the pore space are generally neglected.

The enthalpy can be written to a good approximation

$$q = c_i(T - T_o) + L_o(1 - \phi) \tag{2}$$

where c_i is the volumetric specific heat of ice or snow (or the ice and soil combination for permafrost), L_o is the volumetric latent heat of fusion for ice or snow, and ϕ is the fraction of the volume that is not composed of ice. This includes air- and liquid-filled pore space in the volume, and in frozen ground it also includes the soil or rock matrix. Modern models of snow and frozen soil may allow liquid water to infiltrate and possibly supercool, and therefore additional equations are needed to describe liquid infiltration and the conversion of liquid to ice and vice versa. Such equations may be devised such that the second term in Eq. (2) is not needed. The reader may refer to the Community Land Model, CLM version 4 for a description of one possible model of snow and frozen soil that is designed for a global climate model but is relatively complete [66].

The boundary conditions of Eq. (1) depend on the cryosphere component and possibly the climatic conditions. First consider the special case of floating ice where the basal temperature is always assumed to be at T_f. In these materials, the bottom boundary of Eq. (1) has a temperature boundary condition, and the net flux into the surface excluding the conductive flux in the ice is equal to the heat flux from the water below: $F|_{bottom} = F_W$ (fluxes are taken as positive towards the surface). In contrast, the base of land ice and the lowest point considered in a soil or snowpack model are generally not at the freezing point, in which case Eq. (1) has a flux boundary condition at the base equal to the geothermal heat flux: $F|_{bottom} = F_G$. At the top surface of ice or snow, one must test if the net flux into the top surface can balance the conductive flux (taking z as positive down):

$$F(T)|_{top} = k\frac{\partial T}{\partial z}\bigg|_{top},$$

for a surface temperature below the freezing point ($T < T_f$). If so, then a flux boundary condition is used at that surface in Eq. (1). If the surface temperature is at or above the freezing point, then a temperature boundary condition is used at that surface in Eq. (1) with $T = T_f$.

Conservation of mass

Models of land ice, floating ice, and snow usually employ a fixed number of layers and therefore layer thicknesses vary in time. This so-called moving boundary method requires a Stefan condition to describe ablation, accretion, and accumulation. The rate of change of the top surface position (z_o) for snow or ice is

$$q\,\frac{dz_o}{dt} = F(T)|_{top} - k\frac{\partial T}{\partial z}\bigg|_{top} - S_{fall} + \delta \tag{3}$$

for z_o positive down, where S_{fall} is falling snow, and δ is from snow densification, snow to ice conversion, snow redistribution, etc. The rate of change of the bottom surface position (z_b) for ice is

$$q\,\frac{dz_b}{dt} = -\,F(T)|_{bottom} - k\frac{\partial T}{\partial z}\bigg|_{bottom} \tag{4}$$

for z_b positive down. Land and floating ice must also take into account the horizontal transport of ice, which is described in sections 4 and 5.

Surface energy balance, radiation, surface albedo, and melt ponds

The net flux entering the top surface of land and floating ice, soil, or snow is a sum of radiative and turbulent heat fluxes:

$$F(T)|_{top} = F_r(1 - \alpha) - I_0 + F_L - \epsilon\sigma T^4 + F_s + F_e, \tag{5}$$

where $F_r(1 - \alpha)$ is the net downward solar irradiance above the top surface, α is the surface albedo, I_o is the solar irradiance that penetrates the top surface, F_L is the downward longwave irradiance, $\epsilon\sigma T^4$ is the upward longwave irradiance (for T in Kelvin), ϵ is the emissivity, σ is the Stefan-Boltzmann constant, F_s and F_e are the downward sensible and latent heat fluxes, respectively.

In many ice and snow models, the surface albedo is a function of various quantities such as temperature, snow grain size, snow age, impurities, snow depth, ice thickness, and melt pond coverage. Often shortwave radiation is absorbed in the ice interior based on Beer's law, although Beer's law is inappropriate in materials with depth dependent surface albedo parameterizations. Usually the temperature dependence of the surface albedo is a proxy for modeling melt pond, grain size, and/or surface scattering characteristics. These relatively crude methods are being revamped considerably in models at this time.

A better way is to design a highly interdependent set of physics for radiative transfer, ponding, and liquid infiltration. Ideally one would have radiative transfer account for multiple-scattering and be based on intrinsic optical properties that vary with impurity concentrations, snow grain size, ice bubbles, and brine pockets. Ponds would accumulate water above sea level when there is insufficient hydraulic connectivity to drain meltwater, and they would accumulate below sea level when the hydraulic connectivity is high enough to allow liquid water to rise up from below and flood the surface.

Influence of salts and other impurities

Dissolved impurities such as salts in the pore water depress the freezing point. For ice to remain in local thermodynamic equilibrium, the pore water is always at the freezing point and freezing or melting must occur at the pore-ice interface to dilute or concentrate the solute. If we assume for simplicity that the voids are completely filled with liquid, then the void fraction is a function of temperature and the bulk solute concentration. The solute concentration in the voids, assuming freezing expels the solute completely into the voids, is a function of temperature according to the liquidus relation from the phase diagram of the binary material (ice plus solute). A few global climate models today have sea ice models that allow for such pore-ice interchange (also known as brine pocket physics in sea ice) [54, 55]. However, these models assume the bulk solute concentration is fixed in time, and hence, they neglect the heat and solute transport in the voids. These simplifications made it possible for the first step, but they cannot capture the important structural evolution of young sea ice or rapidly changing permafrost. These processes should not be neglected in models that aim to model biogeochemistry in the polar regions.

4   Land Ice Dynamics

Glaciers are perennial ice masses that are large enough to experience gravitational deformation: the flow of ice under its own weight. Glaciers and ice sheets nucleate where snow accumulation exceeds snow and ice ablation over a period of many years or decades. With time, the accumulated snow is buried and compressed, metamorphosing into firn and then glacier ice. Ice behaves as a nonlinear, visco-plastic fluid; once the ice thickness is sufficient, internal gravitational stresses cause the ice to deform.

Snow accumulation is primarily meteoric (derived from atmospheric precipitation), but snow can also accumulate at a site through wind deposition or avalanching. Ablation refers to the loss of snow and ice through melting, sublimation, wind erosion, or calving, a process where slabs of ice at the glacier margin mechanically fracture and detach from the main ice mass. Iceberg calving is a very effective ablation mechanism for glacier and ice sheets that are in contact with the ocean. Melting occurs at the glacier surface — the ice-atmosphere interface — but there is also melting internally (englacially), at the glacier bed (subglacially), and on vertical ice cliffs that are common at the ice margin, particularly where glaciers reach the sea and a large area of ice can be in contact with water. Melting only leads to ablation in the case where meltwater runs off and is removed from the system; some surface meltwater in the upper regions of glaciers and ice sheets percolates into the snowpack or ponds at the surface, where it can refreeze.

A glacier's mass balance is determined by the net accumulation minus ablation over a specific time period, typically one year. This can be expressed as a total balance ($kg\,yr^{-1}$ or $m^3\,yr^{-1}$ water-equivalent for the entire glacier) or a specific balance, per unit-area of the glacier ($kg\,m^{-2}\,yr^{-1}$ or $m\,yr^{-1}$ water-equivalent). There is no simple 'threshold temperature' for a glacier to be viable; a mean annual temperature below 0°C is not a necessary or sufficient condition for glacier ice to exist. Tidewater glaciers are vivid examples of this. Because ice flow delivers large fluxes of ice to low elevations, glaciers can extend to sea-level environments

where mean annual temperatures are several degrees above 0°C. While most glaciers do not reach the ocean, this feature is intrinsic to all glaciers; glacier ice in the ablation area does not grow *in situ*, but is a consequence of ice transport from the accumulation area to the ablation area.

Glacier flow occurs through three different mechanisms: internal 'creep' deformation, de-coupled sliding at the ice-bed interface, and deformation of subglacial sediments (Figure 1). The former is a function of ice rheology and the stress regime in the ice, while the latter two mechanisms are governed by conditions at the base of the glacier [67]. These processes are described in more detail below.
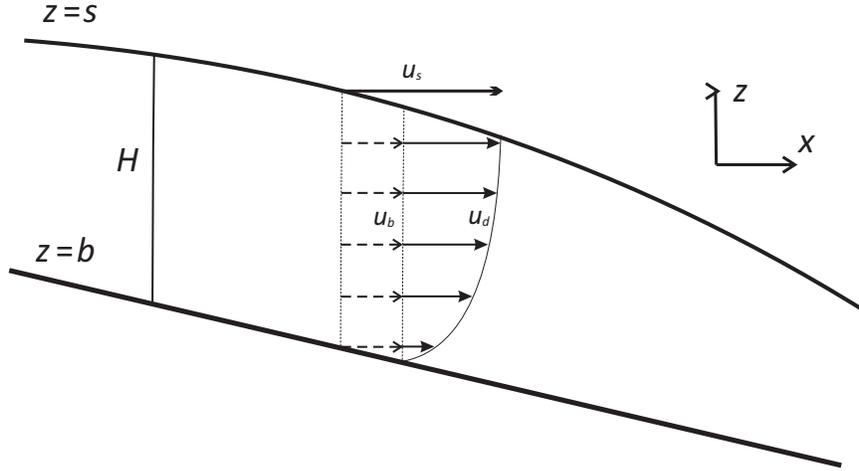

Figure 1: Schematic of glacier flow mechanisms. The surface velocity $u_s = u_b + u_d(s)$. Basal velocity is the sum of deformation of underlying sediments and decoupled sliding at the ice-bed interface. Where ice is moving at the bed, these two processes can operate together, or only one of them may be active.

Governing Equations for Glacier Dynamics

Similar to models of atmosphere or ocean dynamics, the flow of glaciers and ice sheets is mathematically described from the equations for the conservation of mass, momentum, and energy. For a point on the glacier with ice thickness H, the vertically-integrated form of the conservation of mass is most commonly employed in glaciological models:

$$\frac{\partial H}{\partial t} = -\nabla \cdot (\overline{\mathbf{u}} H) + b \,. \tag{6}$$

Here $\overline{\mathbf{u}}$ is the average horizontal velocity in the vertically-integrated ice column and b is the mass balance rate. The first term on the right-hand-side describes the horizontal divergence of ice flux, while the second term describes the net local source or sink of mass associated with accumulation and ablation. The vertically-averaged velocity includes ice flow due to both internal deformation and basal flow: $\overline{\mathbf{u}} = \overline{\mathbf{u_d}} + \mathbf{u_b}$. Glacial ice moves slowly, so a year is typically adopted as the most convenient unit of time; hence, ice velocities are reported in $m\,yr^{-1}$ and b is expressed as $m\,yr^{-1}$ of ice-equivalent gain or loss of mass.

10

The main challenge in modeling glaciers and ice sheet is evaluation of the velocity field. Acceleration and inertial terms are negligible in glacier flow, so the Navier-Stokes equations that describe conservation of momentum reduce to a case of Stokes flow, where gravitational stress is balanced by internal deformation in the ice:

$$\nabla \cdot \sigma = -\rho \mathbf{g}\,, \tag{7}$$

where σ is the ice stress tensor, ρ is ice density, and $\mathbf{g}$ is the gravitational acceleration. Expanding this into the three directional components,

$$\begin{aligned}
\frac{\partial \sigma_{xx}}{\partial x} + \frac{\partial \sigma_{xy}}{\partial y} + \frac{\partial \sigma_{xz}}{\partial z} &= 0\,, \\
\frac{\partial \sigma_{yz}}{\partial x} + \frac{\partial \sigma_{yy}}{\partial y} + \frac{\partial \sigma_{yz}}{\partial z} &= 0\,, \\
\frac{\partial \sigma_{xz}}{\partial x} + \frac{\partial \sigma_{yz}}{\partial y} + \frac{\partial \sigma_{zz}}{\partial z} &= -\rho_i g\,.
\end{aligned} \tag{8}$$

Ice deformation is independent of confining (i.e., hydrostatic) pressure, so ice rheology is usually couched as a function of the deviatoric stress tensor, σ'. Under the assumption that ice is incompressible, the momentum equations can be analyzed to give the horizontal balances

$$\begin{aligned}
2\frac{\partial \sigma'_{xx}}{\partial x} + \frac{\partial \sigma'_{yy}}{\partial x} + \frac{\partial \sigma'_{xy}}{\partial y} + \frac{\partial \sigma'_{xz}}{\partial z} &= -\rho g \frac{\partial h}{\partial x}\,, \\
\frac{\partial \sigma'_{yz}}{\partial x} + 2\frac{\partial \sigma'_{yy}}{\partial y} + \frac{\partial \sigma'_{xx}}{\partial y} + \frac{\partial \sigma'_{yz}}{\partial z} &= -\rho g \frac{\partial h}{\partial y}\,.
\end{aligned} \tag{9}$$

The terms on the right-hand-side represent the surface slope, for the glacier surface $h\,(x,\,y)$. Greve and Blatter [68] present a detailed derivation of this full system of equations and their solution. A constitutive relation is needed to express internal stresses in terms of strain rates in the ice: $\dot{\epsilon}_{ij} = 0.5(\partial u_i/\partial x_j + \partial u_j/\partial x_i)$. Eq. (9) can then be rewritten as a function of the 3D ice velocity field, providing a framework to solve for $\overline{\mathbf{u}}$ and integrate Eq. (6) to model the evolution of glacier geometry in response to variations in ice dynamics or climate. The next section describes the constitutive relation that is most commonly used in glacier modeling.

Because ice rheology is strongly temperature-dependent, an additional equation is needed to solve for the 3D temperature distribution. As discussed in section 3, the local energy balance gives the governing equation for temperature evolution in the ice sheet in Eq. (1).

Given a 3D temperature distribution through the ice sheet, the effective rheology of the ice can be evaluated and the velocity field can be numerically determined. Knowledge of the temperature field is also essential to assessing whether the base of the ice sheet is at the pressure melting point or not; if so, liquid water can be present at the bed and the glacier or ice sheet is subject to basal flow.

Internal Deformation: Ice Rheology

In order to solve the Stokes flow diagnostic equation, ice sheet stresses need to be expressed as velocity fields, via a constitutive relation for ice. The rheology of polycrystalline glacier ice is well-studied in laboratory and field environments [69]. Lab studies of tertiary ice

deformation reveal that ice deforms as a nonlinear viscous fluid [9, 10, 70, 71]. The original form of the flow law proposed by Glen [1955, 1958] is broadly supported by field studies of tunnel and borehole deformation [7, 72], as well as observations and modeling of large-scale ice motion [73, 74].

This constitutive relation is known as Glen's flow law and is written as a function of the second invariant of the deviatoric stress tensor, $\Sigma_2' = (\sigma_{ij}' \, \sigma_{ji}')/2$,

$$\dot{\epsilon}_{ij} = B\,(T)\,\Sigma_2'^{(n-1)/2}\,\sigma_{ij}'\,. \tag{10}$$

$B\,(T)$ is an "ice softness" term that follows an Arhennius temperature dependence,

$$B\,(T) = B_0\,\exp\left(\frac{-Q}{RT}\right)\,. \tag{11}$$

B_0 is called the Glen flow-law parameter, R is a constant, and Q is the creep activation energy. Lab and field studies of ice deformation suggest that B_0 can vary by a factor of about 10 [69]. Including the effects of strain-softening and temperature, the effective viscosity of ice varies by several orders of magnitude.

This formulation is an isotropic flow law that allows the first-order effects of ice temperature and deviatoric stress regime to be incorporated in estimates of ice deformation. Ice deformation is typically modeled as an $n = 3$ process. Where shear stress and shear deformation are dominant, as is often the case, this is well-approximated by

$$\dot{\epsilon}_{xz} = B\,(T)\,\sigma_{xz}'^3\,. \tag{12}$$

Glen's flow law is for pure, isotropic ice. There are numerous other complicating factors for ice deformation, such as anisotropic ice fabric [75, 76, 77], the potential impact of grain size, [78, 79] and the presence of impurities and intergranular liquid water content [80]. These effects are not explicitly resolved in ice sheet models, but the flow rate parameter, B_0, is typically tuned to approximate the bulk effects of crystal fabric, grain size, and impurity content.

The strain rates in Eq. (10) or (12) can be expressed as velocity gradients, and then vertically integrated or inverted and substituted into the momentum balance, Eq. (9), to give a set of equations for the horizontal ice velocity. Various numerical solutions to these equations have been adopted in glacier and ice sheet modeling, outlined in more detail in the next section.

Basal Flow

In addition to internal deformation, glacier ice can flow at the base where the bed is at the pressure-melting point, through some combination of subglacial sediment deformation and decoupled sliding over the bed. Large-scale basal flow generally requires pressurized subglacial meltwater, which can lubricate the bed, float the ice, or weaken subglacial sediments. Subglacial hydrology therefore plays a pivotal role in fast-flowing glaciers and ice streams [81, 82]. High subglacial water pressures can decouple the ice from the bed by reducing or eliminating basal friction. On local scales this may not entice a significant ice-dynamical response, as resistive stresses can be taken up at adjacent well-coupled regions of the bed, by

side drag from valley walls or adjacent ice, or by longitudinal stress bridging (upstream and downstream resistance to flow). However, numerous observational studies report occasions where inputs of surface meltwater to the bed overwhelm these resistive stresses and produce localized speedups in valley glaciers, e.g., [83, 84] and in polar icefields [85, 86, 87].

For large-scale ice stream flow or surging of outlet glaciers, subglacial water must occupy a significant portion of the glacier bed, at pressures which are sufficient to drown geologic and topographic pinning points [84, 88]. In this situation, widespread ice bed decoupling can permit high rates of basal flow (100s to 1000s of $\mathrm{m\,yr^{-1}}$) and a regime in which ice fluxes are dominated by basal flow.

In ice sheets that exhibit high rates of basal flow, there is ongoing uncertainty as to the relative importance of sliding flow along the ice bed interface vs. deformation of the underlying glacial sediment. High subglacial water pressures are conducive to both processes. Fast flow in West Antarctica's Siple Coast ice streams is associated with plastic failure of a thin layer of saturated marine sediment [89, 90], and similar processes are expected to be important wherever subglacial sediments and topographic features offer a relatively smooth, low-friction substrate [91].

Models make some allowance for basal flow, usually through a local sliding 'law' relating basal flow, u_b, to gravitational shear stress at the bed, raised to some power m, $u_b \propto \tau_d^m$. In some applications the effects of subglacial water pressure on basal flow are introduced, typically through the effective pressure p_e. This is the difference between glaciostatic (ice) pressure and subglacial water pressure: $p_e = p_i - p_w$. An effective pressure of 0 indicates that ice is floating, so low or negative effective pressures promote ice-bed decoupling and enhanced basal flow. While it is safe to assume that $u_b \propto p_e^{-k}$, for some unknown power k, there is likely no generalized local relationship between u_b and p_e; actual basal flow is affected by regional-scale ice dynamics, not just local conditions. A prescription of the form $u_b = A\tau_d^m/p_e^k$ is unstable as this blows up as $p_e \to 0$. Local flotation is commonly observed in nature, so $p_e = 0$ is a physically acceptable possibility. The mathematical instability is simply a failure of the local form of the basal flow law. An alternative is to introduce a parameterization in terms of the flotation fraction p_w/p_i, with $u_b = 0$ when $p_w = 0$ and basal flow increasing with p_w/p_i. The local expression $u_b = A\tau_d^m f(p_w/p_i)$ can represent this, e.g., [92]. Basal flow observations are notoriously difficult to make so there is no clear recommendation as to the functional form of $f(p_w/p_i)$. Hydrological enabling of basal flow is expected to be a nonlinear, threshold process [93].

Modeling Glaciers and Ice Sheets

This section describes the physical approximations and numerical techniques in place for simulations of glacier and ice sheet dynamics, based on solution to Eqs. (6), (9), and (1).

One common reduction in ice sheet modeling, known as the shallow-ice approximation, involves a number of scaling assumptions that are valid when horizontal gradients in ice thickness and velocity are small and ice flows dominantly by vertical shear deformation.

Under these conditions, Eq. (9) simplifies to

$$\frac{\partial \sigma'_{iz}}{\partial z} = -\rho g\, \frac{\partial h}{\partial x_i}\,. \tag{13}$$

where subscript i refers to the horizontal direction of interest (x, y). Eq. (13) can be vertically integrated to give

$$\sigma'_{iz}(z) = -\rho g\,(h - z)\,\frac{\partial h}{\partial x_i}\,. \tag{14}$$

This vertical shear stress is commonly known as the gravitational driving stress, τ_d. It vanishes at the glacier surface $(z = h)$ and $\tau_d = -\rho g\, H \nabla h$ at the glacier bed. Substituting for the strain rates based on Glen's flow law and representing strain rates in terms of velocity gradients gives

$$u_i(z) = u_{bi} - 2\,(\rho g)^n\, |\nabla h|^{n-1}\, \frac{\partial h}{\partial x_i} \int_b^z B\,(T)\,(h - z)^n\, dz\,, \tag{15}$$

for basal velocity $\mathbf{u_b}$.

For the shallow-ice approximation represented in Eq. (15), the vertically-averaged ice velocity due to deformation is nonlinearly proportional to local surface slope and ice thickness,

$$\mathbf{u_d} \propto (\nabla h)^n\, H^{n+1}\,. \tag{16}$$

This treatment of ice dynamics has been adopted in most ice sheet modeling studies to date, e.g., [19, 20, 94]. The nonlinearity of Glen's flow law gives ice deformation rates that are exceptionally sensitive to the glacier thickness and surface slope. Under this approximation, ice velocity is solely a function of local ice geometry. This neglects 'farfield' effects and other complicating influences on ice flow, such as longitudinal stretching/compression of the ice and horizontal shearing due to the friction of valley walls. The influence of longitudinal stress coupling on ice dynamics is significant in complex terrain such as valley glaciers and mesoscale icefields [95, 34]. It is also important in settings such as tidewater glaciers, ice shelves, ice streams, transition regions from inland to floating ice dynamics, and ice sheet divides [14, 28]. Many of the most interesting questions in ice sheet behavior involve these parts of the system, so more complete representations of ice dynamics are of great interest.

Doug MacAyeal [1989, 1995] introduced an approximation for ice shelf and ice stream flow that is essentially the complement of the shallow-ice approximation in Eq. (13). Because flow in ice streams is predominantly at the base, a plug-flow approximation, assuming no vertical shear, is reasonable. The gravitational driving stress is then taken up by longitudinal stress, horizontal shear stress, and basal friction. In ice shelves the basal traction also vanishes. Under this approximation, Eq. (9) can be written

$$\begin{aligned}
\frac{\partial}{\partial x}\,(2\,\sigma'_{xx} + \sigma'_{yy}) + \frac{\partial}{\partial y}\,(\sigma'_{xy}) &= -\rho g \frac{\partial h}{\partial x}\,, \\
\frac{\partial}{\partial x}\,(\sigma'_{xy}) + \frac{\partial}{\partial y}\,(\sigma'_{xx} + 2\,\sigma'_{yy}) &= -\rho g \frac{\partial h}{\partial y}\,.
\end{aligned} \tag{17}$$

14

Substituting for strain rates and defining an effective viscosity μ_e from the inverted form of Glen's flow law [16],

$$
\begin{aligned}
\frac{\partial}{\partial x}\left[\mu_e\left(2\frac{\partial u}{\partial x}+\frac{\partial v}{\partial y}\right)\right]+\frac{\partial}{\partial y}\left[\frac{\mu_e}{2}\left(\frac{\partial u}{\partial y}+\frac{\partial v}{\partial x}\right)\right]&=-\rho g\frac{\partial h}{\partial x}, \\
\frac{\partial}{\partial x}\left[\frac{\mu_e}{2}\left(\frac{\partial u}{\partial y}+\frac{\partial v}{\partial x}\right)\right]+\frac{\partial}{\partial y}\left[\mu_e\left(\frac{\partial u}{\partial x}+2\frac{\partial v}{\partial y}\right)\right]&=-\rho g\frac{\partial h}{\partial y}.
\end{aligned}
\tag{18}
$$

A vertically-integrated form of Eq. (18) is readily derived under the assumption that there is no vertical variation in strain rates. These equations can be numerically solved to give the horizontal velocity fields, subject to prescription of a basal shear stress as a boundary condition at the bed.

This set of equations provides a good representation of ice dynamics where vertical shear deformation is negligible. MacAyeal and colleagues have had good success in simulating Antarctic ice stream and ice shelf dynamics with this method. This approach to modeling ice dynamics has also been applied to former ice streams in the Laurentide Ice Sheet [96] and in studies of the inland propagation of ice-marginal thinning in the Amundsen Sea sector of West Antarctica [31]. Using control theory (inverse methods), these equations also provides an opportunity to construct the basal friction from known surface velocity fields [97, 98].

The assumptions that underlie both shallow-ice models and the 'plug-flow' equations are limiting in mixed flow regimes where vertical and horizontal shear stresses and longitudinal stresses are all important. This is the case where ice flow goes through a transition from grounded to floating conditions (the grounding line), where there are large spatial gradients in basal flow, at ice divides, and in valley glaciers, where the shallow-ice approximation is not valid because the ice thickness is of similar magnitude to horizontal variations in ice thickness and velocity. To address this and provide a modeling framework that is generic and self-consistent for all environments, recent efforts have explored solutions to the full Stokes system, Eq. (8), as well as intermediate stages of complexity between the shallow-ice approximation and the full Stokes solution. The development of theoretical and numerical solutions of full stress-field solutions is promising, and has become tractable on regional scales [28, 29, 32]. Full solutions are still computationally unwieldy on continental scales, and have yet to be applied to whole ice-sheet simulations in Greenland or Antarctica.

Progress has been slower in numerical simulations of the subglacial geological and hydrological processes that give rise to basal flow. This remains absent or oversimplified in models, where basal sliding is often specified as a function of gravitational driving stress, subject to thermal regulation. Warm-based ice can slide, while ice frozen to the bed is subject to a no-slip boundary condition. Some recent efforts include explicit models of subglacial water flow and storage, permitting sliding-law formulations that model this control on basal flow [99, 100, 101], but the physical understanding and the numerical representation of these processes remain limited.

Computational Considerations

For whole-ice-sheet simulations, the horizontal grid spacing is typically 20 to 50 km, with some 30 layers in the vertical. Recent simulations have adopted grid sizes of 5 to 10 km. Such

resolutions are tractable but the computational demand increases by an order of magnitude for each factor of two reduction in the resolution, due to a fourfold increase in grid cells and the necessary reduction in the solution time step.

Part of the computational challenge for full-stress solutions arises from the need for long spinup simulations for the polar ice sheets. Both Greenland and Antarctica contain ice that is more than 200 kyr old, and it is essential to model the temperature and thickness evolution of the ice sheets through the last one or two glacial cycles in order to provide a reasonable internal temperature field for present-day studies or future projections of the ice sheets. Present-day dynamical adjustments are ongoing from the longterm evolution of the ice sheets, and this provides a background signal that must be understood in order to evaluate the response of the ice sheets to recent climate change. Regions of the ice sheets are thickening and thinning as a result of the ice sheet and climate history, largely associated with the long timescales of thermal advection and diffusion. The ice sheets are also adjusting to the geometric changes that attended the last deglaciation, e.g., [102]. These 'secular' effects are further compounded by the slow (10^3 to 10^4 year) timescale of isostatic adjustment to the last glacial maximum and the subsequent deglaciation, which also needs to be simulated for the ice sheet system.

Finite difference and finite element approaches have both been applied to glacier and ice sheet models. Finite elements are more versatile and applicable to the complex geometry of mountain glaciers and fixed, limited spatial domains such as ice shelves, and these have advantages for solution of the diagnostic equations for ice velocity. Time-adaptive, moving grids are needed to simulate the evolution of glacier geometry, however, and this combines with the simplicity of finite-difference methods to make these more popular for simulation of large-scale ice sheet dynamics.

Priorities and Challenges

Fundamental glaciological data are still sparse in large sectors of the polar ice sheets and mountain glaciers, including knowledge of ice thickness, thermal regime, and subglacial conditions. It is difficult to apply hydrological and basal flow models to much of Greenland and Antarctica, where groundwater drainage, sediment properties, and other details of the subglacial environment are poorly known. Better understanding of the essential subglacial processes physics is also needed [67], as well as methods to parameterize these subgrid-scale processes in large-scale models. Similar physical and numerical challenges are involved in simulation of iceberg calving; there is no established 'calving law', as the underlying physics and environmental controls are not fully understood.

There is a recent emphasis on glacial systems modeling, including subglacial processes and hydrological evolution, e.g., [93], but these efforts are still in early stages. With these limitations in mind, there is potential for major progress on at least two fronts based on what is currently well-understood about glaciers and ice sheets: (i) through high-resolution, full-Stokes solutions, which are on the horizon, and (ii) through improved coupling of ice sheet and climate models. Improved coupling with climate models is necessary and many research groups have initiated this effort in recent years, for both individual glaciers [103] and continental ice sheets [104, 25, 105, 106].

Improved representation of stress-strain regimes at ice sheet margins, within floating ice and grounding zones, and in drainage basins that feed fast-moving outlets will provide a better representation of interannual and decadal variability of the ice sheets. This will also improve model capability in simulating glacier and ice sheet sensitivity to climate change. Resolutions (and input bedrock and climate-forcing datasets) of order 1 km are needed for this advance in the polar ice sheets, at least in the areas of complex flow and steep gradients at the ice sheet margin. For valley glaciers, input fields and ice dynamics need to be simulated at resolutions of order 100 m, and closer to 10 m if one wishes to simulate interannual glacier terminus response to climate change. It is also important to recognize that even with full-Stokes solutions, ice streams, surging behavior, summer speedups, ice shelf instabilities, and areas of fast flow within the ice sheets will not spontaneously arise in the correct places; these are associated with processes and forcings that are absent in most models. In particular, there is limited two-way interaction between oceans and ice sheets in modeling studies to date, despite recent evidence that ice sheets are highly responsive to ocean warming [107].

5   Floating Ice Dynamics

State of the art climate models today treat the jumble of floating ice floes as a continuum. At present, in global models, the only floating ice with dynamics is sea ice, as lake and river ice models are generally thermodynamic only. There are specialized models of lakes and rivers, and they are based on the same principles as sea ice models, so we discuss their dynamics together here.

The physics of floating ice is strongly dependent on the thickness. Therefore, floating ice is generally described in terms of a distribution of ice thicknesses at the subgrid-scale. The ice motion is also considered for a continuum, rather than for individual floes. With this brief overview, a global-scale floating ice model can be developed from the description of thermodynamics given in section 3 and the additional governing equations for the dynamics and ice-thickness distribution given in this section.

Ice-thickness distribution

The formulation of a floating ice model begins with the ice-thickness distribution equation. The ITD is a probability density function (pdf), usually written $g(h)$, that describes the probability that the ice cover in a particular region has thickness h. A cruder alternative is to model the mean thickness of the pdf and the total ice concentration.

In a floating ice model, the ITD describes the pdf of a grid cell and thus it is sometimes called a subgrid-scale parameterization. A parameterization typically represents processes that are too small-scale or complex to be represented explicitly. For example, deformation is parameterized with a set of rules in a continuum model because there is no known differential equation that describes deformation in this type of model. The rules must select the portion of the ITD that will deform and then redistribute it within the ITD. In contrast, ice growth and melt alter the ITD in a way that is computed from first principles. Hence the ITD actually includes both parameterized and explicit physics.

The ITD equation is

$$\frac{Dg}{Dt} = -g\nabla \cdot \mathbf{u} + \Psi - \frac{\partial}{\partial h}(fg) + \mathcal{L} \tag{19}$$

where the left hand side is the Lagrangian derivative of g following an ice "parcel" and terms on the right hand side are the rate of change of g from parcel convergence, mechanical redistribution (Ψ, see Fig. 2), advection of g in ice-thickness space from growth/melt (see Fig. 3), and the reduction rate of g from lateral melt ($\mathcal{L}$). Here, $\mathbf{u}$ is the horizontal ice velocity (vertical ice velocity is ignored) and f is the net growth rate. The ITD equation was introduced by [44]. Models that specify the ITD, e.g., [108], or only permit a single ice thickness in the ice covered fraction of a model grid cell, e.g., [109], would have an equation for the gridcell mean ice thickness instead.
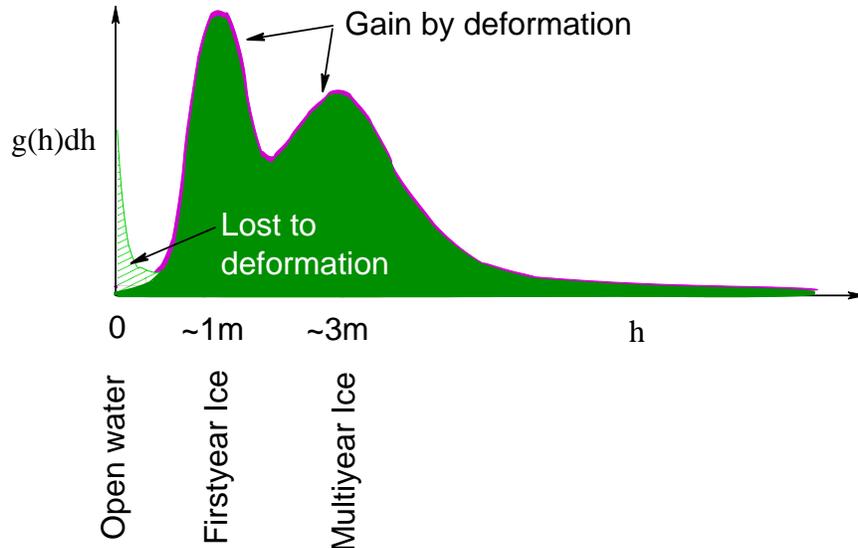

Figure 2: Illustration of deformation. The portion of the distribution labeled "lost to deformation" is also known as the ice that participates in redistribution. It subsequently is redistributed to thicker parts of $g(h)$, where it is labeled "gain by deformation".

There are two parts to deformation: a rate of opening (creating open water) and closing (closing open water and/or deforming and redistributing the ice), which depend on $\mathbf{u}$ and $g(h)$. The opening and closing rates depend on the convergence and/or shear in the ice motion field. It may not be obvious that shear would cause deformation. Imagine that the ice pack is composed of pieces with jagged edges. When shearing, the jagged edges can catch on one another and cause deformation, which converts kinetic energy into potential energy from piling up ice, or shearing can cause frictional loss of energy and no deformation. Thus the closing rates also depend on assumptions made about frictional losses, see e.g., [51, 54].

A mathematical representation of lead opening and mechanical redistribution is most conveniently written in terms of the divergence and shear of $\mathbf{u}$, $\dot{\epsilon}_I$ and $\dot{\epsilon}_{II}$, respectively. The parameterization follows from [44]:

$$\Psi = |\dot{\epsilon}|[\alpha_0(\theta)\delta(h) + \alpha_r(\theta)w_r(h, g)], \tag{20}$$

where $|\dot{\epsilon}| = (\dot{\epsilon}_I^2 + \dot{\epsilon}_{II}^2)^{1/2}$, $\theta = \tan^{-1}(\dot{\epsilon}_{II}/\dot{\epsilon}_I)$, $\delta(h)$ (the delta function) is the opening mode and $w_r(h, g)$ is the ridging mode. The coefficients $|\dot{\epsilon}|\alpha_0(\theta)$ and $|\dot{\epsilon}|\alpha_r(\theta)$ are known as the
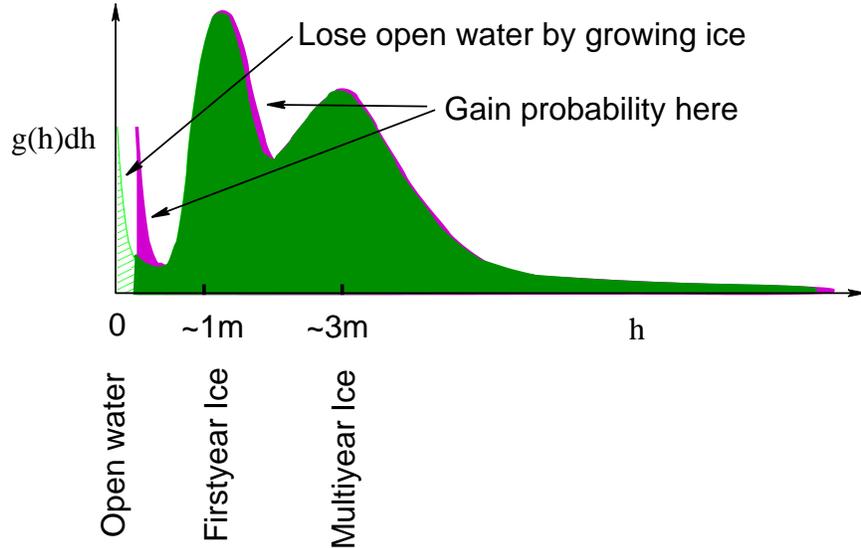
Figure 3: Illustration of advection in thickness space.

lead opening and closing rates, respectively, and they are related such that their difference equals the divergence, $|\dot{\epsilon}|\alpha_0(\theta) - |\dot{\epsilon}|\alpha_r(\theta) = \dot{\epsilon}_I$.

For the redistribution process, some portion of $g(h)$ is identified as potentially able to "participate" in redistribution (see Fig. 2). This is usually the thinnest 15% of $g(h)$. If the open water fraction exceeds 15%, then no redistribution takes place, and instead the open water closes under convergence and nothing happens under shear. The so called participation function is weighted according to its thickness, so that the thinnest ice is most likely to deform. Then a rule is needed to redistribute the ice that ridges. Originally, [44] proposed that ridged ice would end-up five times thicker than its starting thickness. Other more complex redistribution schemes have been used since then [43, 110]. The interested reader can refer to these references for examples of parameterizations for $w_r(h, g)$.

The other primary mechanism that changes $g(h)$ is ice growth or melt, which cause $g(h)$ to shift in thickness space. This process is illustrated in Fig. 3. The growth/melt rate depends on thickness, so $g(h)$ becomes distorted in the process.

An explicit conservation equation for ice volume (or mass) is not given in this section because conservation of volume is contained in the equation for $g(h)$ (or at least it depends on the way $g(h)$ is discretized).

Momentum equation

The second governing equation is conservation of momentum:

$$m\frac{D\mathbf{u}}{Dt} = -m f \mathbf{k} \times \mathbf{u} + \boldsymbol{\tau}_{\mathrm{a}} + \boldsymbol{\tau}_{\mathrm{w}} - mg_{\mathrm{r}}\nabla Y + \nabla \cdot \sigma, \qquad (21)$$

where the left hand side is the Lagrangian derivative of $\mathbf{u}$ following an ice parcel, the right hand side begins with a term representing Coriolis force, air and water stresses, the force

19

due to ocean surface tilt, and the ice internal force. In this equation m is mass per unit area, f is the Coriolis parameter, g_r is gravity, Y is the sea surface height, and σ is the ice stress.

Ice rheology and the constitutive law

A constitutive law characterizes the relationship between the ice stress and strain rate and defines the nature of the ice dynamics. A simplistic picture of a converging ice pack with uniform thickness under an imposed compressive wind force is given in Fig. 4. Floating ice generally repels the compressive force somewhat even if it is deforming. The resulting internal force is associated with a nonzero stress state. In Fig. 4 the ice pack is converging such that its length L on one side decreases by δL in some time δt, so the ice experiences a strain $\epsilon = \delta L / L$ and a strain rate $\dot{\epsilon} = \delta L / L \delta t$. A modeler chooses the constitutive law to relate σ and $\dot{\epsilon}$, which are actually two-dimensional tensors, not scalars as shown in Fig 3 for illustrative purposes only. In two dimensions, the divergence and shear of the ice velocity can be conveniently used to describe the strain rate tensor as they are invariant across grid transformations.

Initial state

Ice slab side view

length L

After applying a converging wind stress for time δt

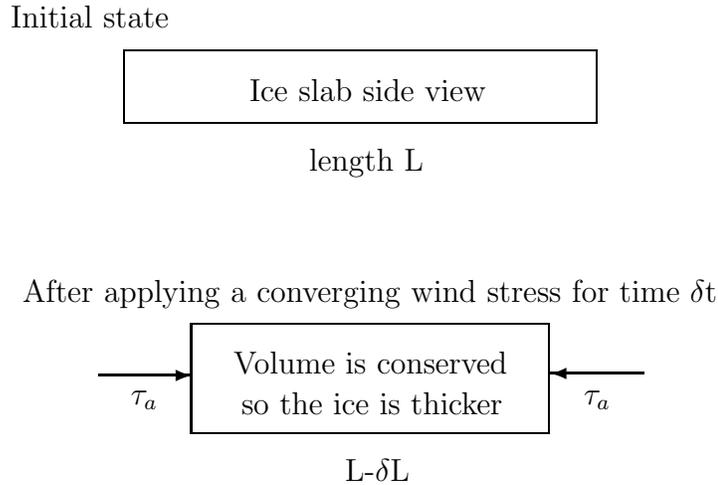τ_a → Volume is conserved so the ice is thicker ← τ_a

L-δL

Figure 4: Illustration of ice slab that deforms under compressive force.

The momentum equation depends on the ice internal force, which in turn depends on the ice stress tensor. The most common rheology used today is the viscous-plastic rheology from [109] (or a close derivative thereof) where the ice behavior is plastic at normal strain rates and viscous at very small strain rates.

The constitutive law for the viscous-plastic model of floating ice can be cast in terms of the invariants of stress (σ_I and σ_{II}) and strain rate ($\dot{\epsilon}_I$ and $\dot{\epsilon}_{II}$) with the pair of equations

$$
\begin{aligned}
\sigma_I &= \zeta \dot{\epsilon}_I - P/2 \\
\sigma_{II} &= \eta \dot{\epsilon}_{II},
\end{aligned}
\tag{22}
$$

where P is the ice strength and ζ and η are bulk and shear viscosities, respectively. The relationship between the viscosities and strain rate invariants is chosen so that the stress

20

state lies on an elliptical yield curve,

$$\frac{(\sigma_I + P/2)^2}{(P/2)^2} + \frac{\sigma_{II}^2}{(P/2e)^2} = 1, \tag{23}$$

where e is the ratio of the principal axes of the ellipse (the original Hibler model [109] used $e = 2$, which is still common today). Thus requiring

$$\begin{aligned}
\zeta &= \frac{P}{2\Delta} \\
\eta &= \frac{\zeta}{e^2} \\
\Delta &= \left(\dot{\epsilon}_I^2 + \dot{\epsilon}_{II}^2 e^{-2}\right)^{1/2}
\end{aligned} \tag{24}$$

for plastic behavior. To avoid infinite viscosities as $\Delta \to 0$, ζ and η are assigned large constant values. In this case the stress state lies inside the elliptical yield curve and the ice behaves like a viscous fluid, exhibiting creep.

The ice strength must be parameterized somehow. For a model with ridging, P can be based on the energetics argument proposed by [111] for plastic deformation, where the compressive strength is equated to the potential energy increase per unit strain in pure convergence. Following [43], the potential energy is multiplied by a constant to account for the dissipation of kinetic energy by frictional energy loss during ridging,

$$P = ZC_p \int_0^\infty h^2 w_r(h) dh \tag{25}$$

where $C_p = 0.5(\rho_i/\rho_w)\hat{g}(\rho_w - \rho_i)$ and Z is the ratio of total energy dissipated to potential energy gain (ρ_i and ρ_w are the densities of ice and water and $\hat{g}$ is the acceleration due to gravity). [112] and [113] recommend $Z = 17$.

Computational Considerations

Computation time given to the sea ice component of a typical global climate models is roughly 10-20% for a $\sim$100 km resolution ice grid, although it could easily be more or less depending on the relative resolution, sophistication, and optimization among components. Lake and river ice in global climate models take a trivial portion of the total computation time because their area is so small compared to the rest of the globe.

A key consideration for climate modelers is to design a model that can run the scenarios of interest in a time to meet publication deadlines. Choices must be made to balance model resolution, physics, parameterizations, and numerics. High performance computers today have tens of thousands of cores and many have been constructed for the purpose of running climate models. Codes must parallelize well to take advantage of these machines, and sea ice codes generally do because there are relatively many processes that operate at the grid-scale (e.g., vertical heat equation) and subgrid-scale (e.g., deformation). The Los Alamos Sea Ice model CICE has already been successfully scaled beyond 10,000 cores on Cray XT equipment [114].

6 Future Directions

Most of the progress to date in modeling glaciers, ice sheets, permafrost, and snow science has stemmed from independent efforts by individual researchers. Advances have paralleled the much larger, coordinated research programs dedicated to the development of climate models, with little crossover or integration. This contrasts with modeling developments in sea ice studies, which are now fully integrated in most ocean-atmosphere general circulation models.

To date there have been few efforts to couple climate and ice sheet models. Most ice sheet simulations use 'offline' forcing where climate model derived fields are used to drive simulations of ice sheet evolution, through one-way forcing. The long timescale of ice sheet evolution means that this may be a reasonable approach, but evolution of ice sheet albedo and topography feeds back on atmospheric conditions on timescales of decades to millennia. Further, there are direct seasonal-timescale links between climate and the dynamics of glaciers and ice sheets, including the effects of surface meltwater and a possible link between coastal ocean temperature and sea ice conditions and outlet-glacier dynamics. These processes all require improved coupling between climate and ice sheet models. This is particularly true at the ice-ocean interface, where mass and energy exchanges are not physically modeled in current simulations.

In general the mass balance fields (accumulation – melt) simulated by climate models are not accurate enough for fully coupled ice sheet-climate modeling, nor can sophisticated atmospheric models be integrated over the millennial time scales of interest for ice sheet evolution. However, the development of improved regional-scale meteorological and glacier mass balance models, e.g., [115, 116, 117], permit direct estimates of surface mass balance from meteorological models, and offer a good physically-based method to simulate how these fields can be expected to change with ice sheet geometry.

The challenge is greater for the mass balance fields and surface climatological forcing of mountain glaciers and permafrost. Mountain glaciers reside in complex terrain where temperature and precipitation gradients are steep. The topography and relevant meteorological processes are not faithfully resolved in even regional climate models, so some form of climatic downscaling is needed to prescribe mass balance fields for glacier modeling [103]. These methods generally do not conserve energy or mass, and improved treatments are needed. There are different considerations for permafrost modeling, but they also relate to the resolution of the landscape and surface climate. The mean annual surface temperature that governs permafrost aggradation and degradation depends on local-scale vegetation, snowpack depth, hydrology, and soil properties, which commonly vary over a spatial scale of meters. Hence, global-scale permafrost and snow models should be interpreted 'statistically' for a region (i.e. via a distribution of permafrost thickness and snow depth in a given climate-model grid cell, based on the range of ground cover and snow conditions in the region).

In contrast to the terrestrial components of the cryosphere, the needs of global climate models often drive sea ice model developments. For example, models that use eddy-resolving ocean components are approaching the large floe-scale, where sea ice (assumed to be on the same grid) can no longer be considered a continuum. Rheologies that attempt to treat ice as a granular material hold promise as a means to extend the utility of continuum models to

smaller length scales. Such rheologies often use Mohr-Coulomb or decohesive type yield curves, which depart from the standard elliptical yield curve particularly where the stress states on the ellipse resist breaking under tension. The floe models to date do well at modeling deformation but the process of joining floes at freeze-up has not been solved [112, 118].

Recent observations of sea ice reveal very long, narrow openings, or leads, in the ice that suggest oriented weaknesses occur. These regions have been dubbed linear kinematic features [119]. Such features occur in sea ice models with isotropic rheologies, such as the viscous-plastic type, with some level of realism at fine resolution [120]. However, models that account for such anisotropy explicitly by keeping track of lead orientation and computing resistance to opening depending on the orientation with respect to leads, e.g., [121, 122], may be able to match observations better [123].

The drive to model the carbon cycle and hence ecosystem dynamics in global climate models has spawned an effort to model sea ice algae and nutrient cycling. When seawater freezes, algae stick to the ice particles, and as the ice particles combine they trap brine, nutrients, and organisms in brine pockets. Biomass concentrations can be hundreds of times greater in sea ice than in seawater, and carbon and key nutrients in sea ice are a substantial fraction of the total in ice-covered regions. When sea ice melts it deposits these materials into the ocean precisely when solar input and meltwater runoff is highest, creating prime conditions for an ocean bloom. Models of these processes have been developed offline [124, 125, 126, 127, 128] and will soon be implemented in sea ice models of global climate models. Models of ecosystem dynamics in sea ice also require a treatment of seawater infiltration, brine drainage, and meltwater flushing, which necessarily involves modeling sea ice salinity [128].

Modeling the cryosphere today is concerned with far more than describing Earth's surface albedo. Global climate models need to be coupled to components of the cryosphere with adequate sophistication to investigate modern scientific problems involving sea level rise, Arctic sea ice retreat, permafrost thawing, and more. There is also evidence that models with better physics are among the models that agree best with observations [129].

References

[1] Lemke, P, Ren, J, Alley, R. B, Allison, I, Carrasco, J, Flato, G, Fujii, Y, Kaser, G, Mote, P, Thomas, R. H, & Zhang, T. (2007) *Observations: changes in snow, ice and frozen ground. In Climate Change 2007: the Physical Science Basis. Contribution of Working Group I to the fourth assessment report of the Intergovenmental Panel on Climate Change*, eds. Solomon, S, Qin, D, Manning, M, Chen, Z, Marquis, M, Averyt, K, Tignor, M, & Miller, H. (Cambridge University Press, Cambridge, UK), pp. 337–384.

[2] Fetterer, F, Knowles, K, Meier, W, & Savoie, M. (2002) Sea Ice Index. National Snow and Ice Data Center. Digital media., updated 2009.

[3] Budyko, M. I. (1969) The effect of solar radiatin variations on the climate of the earth. *Tellus* **21**, 611–619.

[4] Sellers, W. D. (1969) A global climate model based on the energy balance of the earth-atmosphere system. *J. Appl. Meteor.* **8**, 392–400.

[5] Manabe, S. (1969) Climate and the ocean circulation i. the atmospheric circulation and the hydrology of the earth's surface. *Mon. Wea. Rev.* **97**, 739–774.

[6] Bryan, K. (1969) Climate and the ocean circulation iii. the ocean model. *Mon. Wea. Rev.* **97**, 806–827.

[7] Nye, J. F. (1953) The flow law of ice from measurements in glacier tunnels, laboratory experiments, and the jungfraufirn borehole experiment. *Proc. Royal Soc. London, Series A* **219**, 477–489.

[8] Nye, J. F. (1957) The distribution of stress and velocity in glaciers and ice sheets. *Proc. Royal Soc. London, Series A* **275**, 87–112.

[9] Glen, J. W. (1955) The creep of polycrystalline ice. *Proc. Royal Soc. London, Series A* **228**, 519–538.

[10] Glen, J. W. (1958) The flow law of ice. a discussion of the assumptions made in glacier theory, their experimental foundations and consequences. *Int. Assoc. Hydrol. Sci. Publ.* **47**, 171–183.

[11] Budd, W. F. (1970) The longitudinal stress and strain-rate gradients in ice masses. *J. Glaciol.* **9**, 29–48.

[12] Mahaffy, M. W. (1976) A three-dimensional numerical model of ice sheets: tests on the barnes ice cap, northwest territories. *J. Geophys. Res.* **81**, 1059–1066.

[13] Jenssen, D. (1977) A three-dimensional polar ice sheet model. *J. Glaciol.* **18**, 373–389.

[14] Raymond, C. F. (1983) Deformation in the vicinity of ice divides. *J. Glaciol.* **29**, 357–373.

[15] Thomas, R. A & MacAyeal, D. R. (1982) Derived characteristics of the ross ice shelf, antarctica. *J. Glaciol.* **28 (100)**, 397–412.

[16] MacAyeal, D. R. (1989) Large-scale flow over a viscous basal sediment: Theory and application to ice stream b, antarctica. *J. Geophys. Res.* **94 (B4)**, 4071–4088.

[17] Huybrechts, P & Oerlemans, J. (1988) Evolution of the east antarctic ice sheet: a numerical study of thermo-mechanical response patterns with changing climate. *Ann. Glaciol.* **11**, 52–59.

[18] Huybrechts, P. (1990) A 3-d model for the antarctic ice sheet: a sensitivity study on the glacial-interglacial contrast. *Clim. Dyn.* **5**, 79–82.

[19] Huybrechts, P, Letréguilly, A, & Reeh, N. (1991) The greenland ice sheet and greenhouse warming. *Palaeogeography, Palaeoclimatology, Palaeoecology* **89 (4)**, 399–412.

[20] Huybrechts, P & de Wolde, J. (1999) The dynamic response of the greenland and antarctic ice sheets to multiple-century climatic warming. *J. Climate* **12**, 2169–2188.

[21] Huybrechts, P, Janssens, I, Poncin, C, & Fichefet, T. (2002) The response of the greenland ice sheet to climate changes in the 21st century by interactive coupling of an aogcm with a thermomechanical ice-sheet model. *Ann. Glaciol.* **35**, 409–415.

[22] Huybrechts, P, Gregory, J, Janssens, I, & Wild, M. (2004) Modelling antarctic and greenland volume changes during the 20th and 21st centuries forced by gcm time slice integrations. *Global and Planetary Change* **42**, 83–105.

[23] MacAyeal, D. R, Rommelaere, V, Huybrechts, P, Hulbe, C. L, Determann, J, & Ritz, C. (1996) An ice-shelf model test based on the ross ice shelf. *Ann. Glaciol.* **23**, 46–51.

[24] Payne, A. J, Huybrechts, P, Abe-Ouchi, A, Calov, R, Fastook, J. L, Greve, R, Marshall, S. J, Marsiat, I, Ritz, C, Tarasov, L, & Thomassen, M. P. A. (2000) Results from the eismint model intercomparison: the effects of thermomechanical coupling. *J. Glaciol.* **46 (153)**, 227–238.

[25] Ridley, J. K, Huybrechts, P, Gregory, J, & Lowe, J. (2005) Elimination of the greenland ice sheet in a high co_2 climate. *J. Climate* **18**, 3409–3427.

[26] Driesschaert, Fichefet, E. T, Goosse, H, Huybrechts, P, Janssens, I, Mouchet, A, Munhoven, G, Brovkin, V, & Weber, S. L. (2007) Modeling the influence of greenland ice sheet melting on the atlantic meridional overturning circulation during the next millennia. *Geophys. Res. Lett.* **34**, L10707.

[27] Mikolajewicz, U, Vizcaíno, M, Jungclaus, J, & Schurgers, G. (2007) Effect of ice sheet interactions in anthropogenic climate change simulations. *Geophys. Res. Lett.* **34 (L18706)**, doi:10.1029/2007GL031173.

[28] Pattyn, F. (2003) A new three-dimensional higher-order thermomechanical ice sheet model: basic sensitivity, ice stream development and ice flow across subglacial lakes. *J. Geophys. Res.* **108 (B8)**, 2382, doi:10.1029/2002JB002329.

[29] Pattyn, F, Huyghe, A, Brabander, S. D, & Smedt, B. D. (2006) The role of transition zones in marine ice sheet dynamics. *J. Geophys. Res.* **111 (F02004)**, doi:10.1029/2005JF000394.

[30] Pattyn, F & others, . (2008) Benchmark experiments for higher-order and full stokes ice sheet models (ismip-hom). *The Cryosphere* **2**, 95–108.

[31] Payne, A. J, Vieli, A, Shepherd, A, Wingham, D. J, & Rignot, E. (2004) Recent dramatic thinning of largest west-antarctic ice stream triggered by oceans. *Geophys. Res. Lett.* **31**, L23401.

[32] Price, S. F, Conway, H, Waddington, E. D, & Bindschadler, R. A. (2008) Model investigations of inland migration of fast-flowing outlet glaciers and ice streams. *J. Glaciol.* **54**, 49–60.

[33] Oerlemans, J, Anderson, B, Hubbard, A, Huybrechts, P, Jóhannesson, T, Knap, W. H, Schmeits, M, Stroeven, A. P, van de Wal, R. S. W, Wallinga, J, & Zuo, Z. (1998) Modelling the response of glaciers to climate warming. *Clim. Dyn.* **14**, 267–274.

[34] Blatter, H. (1995) Velocity and stress fields in grounded glaciers: a simple algorithm for including deviatoric stress gradients. *J. Glaciol.* **41**, 333–344.

[35] Albrecht, O, Jansson, P, & Blatter, H. (2000) Modelling glacier response to measured mass balance forcing. *Ann. Glaciol.* **31**, 91–96.

[36] Schneeberger, C, Albrecht, O, Blatter, H, Wild, M, & R, R. H. (2001) Modelling the response of glaciers to a doubling in atmospheric co2: a case study of storglaciaren, northern sweden. *Clim. Dyn.* **17 (11)**, 825–834.

[37] Pattyn, F. (2002) Transient glacier response with a higher-order numerical ice-flow model. *J. Glaciol.* **48 (162)**, 467–477.

[38] Jarosch, A. H. (2008) Icetools: A full stokes finite element model for glaciers. *Computers and Geosciences* **34 (8)**, 1005–1014.

[39] Rutt, I. C, Hagdorn, M, Hulton, N. R. J, & Payne, A. J. (2009) The glimmer community ice sheet model. *J. Geophys. Res.* **114 (F02004)**, doi:10.1029/2008JF001015.

[40] Coon, M. D, Maykut, G. A, Pritchard, R. S, Rothrock, D. A, & Thorndike, A. S. (1974) Modeling the pack ice as an elastic-plastic material. *AIDJEX Bull.* **24**, 1–105.

[41] Coon, M. D. (1980) in *Sea Ice Processes and Models*, ed. Pritchard, R. S. (University of Washington Press).

[42] Hibler, W. D. (1980) in *Sea Ice Processes and Models*, ed. Pritchard, R. S. (University of Washington Press), pp. 163–176.

[43] Hibler, W. D. (1980) Modeling a variable thickness ice cover. *Mon. Wea. Rev.* **108**, 1943–1973.

[44] Thorndike, A. S, Rothrock, D. S, Maykut, G. A, & Colony, R. (1975) The thickness distribution of sea ice. *J. Geophys. Res.* **80**, 4501–4513.

[45] Untersteiner, N. (1961) On the mass and heat budget of arctic sea ice. *Arch. Meteorol. Geophys. Bioklimatol., A* **12**, 151–182.

[46] Maykut, G. A & Untersteiner, N. (1971) Some results from a time-dependent thermodynamic model of sea ice. *J. Geophys. Res.* **76**, 1550–1575.

[47] Semtner, A. J. (1976) A model for the thermodynamic growth of sea ice in numerical investigaions of climate. *J. Phys. Oceanogr.* **6**, 379–389.

[48] Washington, W. M & Meehl, G. A. (1989) Climate sensitivity due to increased CO_2: Experiments with a coupled atmosphere and ocean general circulation model. *Clim. Dyn.* **8**, 211–223.

[49] Manabe, S, Stouffer, R. J, Spellman, M. J, & Bryan, K. (1991) Transcient responses of a coupled ocean-atmosphere model to gradual changes of atmospheric CO_2. Part I. Annual mean response. *J. Climate* **4**, 785–818.

[50] McFarlane, N. A, Boer, G. J, Blanchet, J.-P, & Lazare, M. (1992) The Canadian Climate Centre second-generation general circulation model and its equilibrium climate. *J. Climate* **5**, 1013–1044.

[51] Flato, G. M & Hibler III, W. D. (1992) Modeling pack ice as a cavitating fluid. *J. Phys. Oceanogr.* **22**, 626–651.

[52] Hunke, E. C & Dukowicz, J. K. (1997) An elastic-viscous-plastic model for sea ice dynamics. *J. Phys. Oceanogr.* **27**, 1849–1867.

[53] Zhang, J & Hibler III, W. D. (1997) On an efficient numerical method for modeling sea ice dynamics. *J. Geophys. Res.* **102**, 8691–8702.

[54] Bitz, C. M, Holland, M. M, Weaver, A. J, & Eby, M. (2001) Simulating the ice-thickness distribution in a coupled climate model. *J. Geophys. Res.* **106**, 2441–2464.

[55] Holland, M. M, Bitz, C. M, Hunke, E. C, Lipscomb, W. H, & Schramm, J. L. (2006) Influence of the sea ice thickness distribution on polar climate in CCSM3. *J. Climate* **19**, 2398–2414.

[56] Goodrich, L. E. (1978) *Some results of a numerical study of ground thermal regimes.* Vol. Nat. Res.Counc. of Canada, Ottawa, 29–34, pp. 29–34.

[57] Goodrich, L. E. (1978) Efficient numerical technique for one-dimensional thermal problems with phase change. *Int. J. Heat Mass Transfer* **21**, 615–621.

[58] Jordan, R. (1991) A one-dimensional temperature model for a snow cover, (Cold Regions Research and Engineering Laboratory, Special Report 91-16, 49pp), Technical report.

[59] Loth, B, Graf, H.-F, & Oberhuber, J. M. (1993) Snow cover model for global climate simulations. *J. Geophys. Res.* **98**, 10451–10464.

[60] Douville, H, Royer, J. F, & Mahfouf, J. F. (1995) A new snow parameterization for the meteo-france climate model. 1. validation in stand-alone experiments. *Clim. Dyn.* **12**, 21–35.

[61] Robock, A, Vinnikov, K. Y, Schlosser, C. A, Speranskaya, N. A, & Xue, Y. (1995) Use of midlatitude soil moisture and meteorological observations to validate soil moisture simulations with biosphere and bucket models. *J. Climate* **8**, 15–35.

[62] Yang, Z. L, Pitman, A. J, McAvaney, B, & Sellers, A. H. (1995) The impact of implementing the bare essentials of surface ransfer land surface scheme into the BMRC GCM. *Clim. Dyn.* **11**, 279–297.

[63] Slater, A. G, Pitman, A. J, & Desborough, C. E. (1998) The validation of a snow parameterization designed for use in general circulation models. *Int. J. Clim.* **18**, 595–617.

[64] Slater, A. G, Pitman, A. J, & Desborough, C. E. (1998) Simulation of freeze-thaw cycles in a general circulation model land surface scheme. *J. Climate* **103**, 11,303–11,312.

[65] Dery, S & Tremblay, L.-B. (2004) Modelling the effects of wind redistribution on the snow mass budget of polar sea ice. *J. Phys. Oceanogr.* **34**, 258–271.

[66] Briegleb, B. P, Bitz, C. M, Hunke, E. C, Lipscomb, W. H, & Schramm, J. L. (2010) *Technical description of version 4.0 of the Community Land Model Version (CLM)* (National Center for Atmospheric Research NCAR/TN-478+STR).

[67] Clarke, G. K. C. (2005) Subglacial processes. *Ann. Rev. Earth Planet. Sci.* **33**, 247–276.

[68] Greve, R & Blatter, H. (2009) *Dynamics of Ice Sheets and Glaciers.* (Springer-Verlag, Berlin).

[69] Paterson, W. S. B. (1994) *The Physics of Glaciers, 3rd Ed.* (Elsevier, Amsterdam).

[70] Duval, P. (1981) Creep and fabrics of polycrystalline ice under shear and compression. *J. Glaciol.* **27**, 129–140.

[71] Mellor, M & Cole, D. M. (1982) Deformation and failure of ice under constant stress or constant strain-rate. *Cold Reg. Sci. Tech.* **5**, 201–219.

[72] Hooke, R. L. (1981) Flow law for polycrystalline ice in glaciers: comparison of theoretical predictions, laboratory data, and field measurements. *Rev. Geophys. Space Phys* **19**, 664–672.

[73] Adalgeirsdóttir, G, Gudmundsson, G, & Bj*o*rnsson, H. (2000) The response of a glacier to a surface disturbance: a case study on vatnajkull ice cap, iceland. *Ann. Glaciol.* **31**, 104–110.

[74] Alley, R. B. (1992) Flow-law hypotheses for ice-sheet modelling. *J. Glaciol.* **38**, 245–256.

[75] Shoji, H & Langway, C. C. (1988) Flow-law parameters of the dye 3, greenland, deep ice core. *Ann. Glaciol.* **10**, 146–150.

[76] Thorsteinsson, T, Waddington, E. D, Taylor, K. C, Alley, R. B, & Blankenship, D. D. (1999) Strain-rate enhancement at dye 3, greenland. *J. Glaciol.* **45**, 338–345.

[77] Thorsteinsson, T, Waddington, E. D, & Fletcher, R. C. (2003) Spatial and temporal scales of anisotropic effects in ice-sheet flow. *Ann. Glaciol.* **37**, 40–48.

[78] Cuffey, K. M, Thorsteinsson, T, , & Waddington, E. D. (2000) A renewed argument for crystal size control of ice sheet strain rates. *J. Geophys. Res.* **105 (B12)**, 27,889–27,894.

[79] Durham, W, Stern, L, & Kirby, S. (2001) Rheology of ice i at low stress and elevated confining pressure. *J. Geophys. Res.* **106 (B6)**, 11,031–11,042.

[80] Paterson, W. S. B. (1991) Why ice-age ice is sometimes 'soft'. *Cold Reg. Sci. Tech.* **20 (1)**, 75–98.

[81] Bindschadler, R. A. (1983) The importance of pressurised subglacial water in separation and sliding at the glacier bed. *J. Glaciol.* **29**, 3–19.

[82] Clarke, G. K. C. (1987) Fast glacier flow: Ice streams, surging, and tidewater glaciers. *J. Geophys. Res.* **92**, 8835–8841.

[83] Iken, A & Bindschadler, R. A. (1986) Combined measurements of subglacial water pressure and surface velocity of findelengletscher, switzerland: conclusions about drainage system and sliding mechanism. *J. Glaciol.* **32 (110)**, 101–119.

[84] Kamb, B. (1987) Glacier surge mechanism based on linked cavity configuration of the basal water conduit system. *J. Geophys. Res.* **92 (B9)**, 9083–9100.

[85] Copland, L, Sharp, M. J, & Nienow, P. (2003) Links between short-term velocity variations and the subglacial hydrology of a predominantly cold polythermal glacier. *J. Glaciol.* **49**, 337–348.

[86] Zwally, H. J, an T. Herring, W. A, Larson, K, Saba, J, & Steffen, K. (2002) Surface melt-induced acceleration of greenland ice-sheet flow. *Science* **297**, 218–222.

[87] Joughin, I, Das, S. B, King, M. A, Smith, B. E, Howat, I. M, & Moon, T. (2008) Seasonal speedup along the western flank of the greenland ice sheet. *Science* **320 (5877)**, 781–783.

[88] Alley, R. B. (2000) Water pressure coupling of sliding and bed deformation. *Space Science Reviews* **92**, 295–310.

[89] Kamb, B. (1991) Rheological nonlinearity and flow instability in the deforming bed mechanism of ice stream flow. *J. Geophys. Res.* **96 (B10)**, 16,585–16,595.

[90] Tulaczyk, S. M, Kamb, B, & Engelhardt, H. (2001) Basal mechanics of ice stream b, west antarctica i: Till mechanics. *J. Geophys. Res.* **105 (B1)**, 463–481.

[91] Clark, P. U, Alley, R. B, & Pollard, D. (1999) Northern hemisphere ice-sheet influences on global climate change. *Science* **286**, 1104–1111.

[92] Marshall, S. J, Björnsson, H, Flowers, G. E, & Clarke, G. K. C. (2005) Modeling vatnajökull ice cap dynamics. *JGR* **110 (F03009)**, doi: 10.1029/2004JF000262.

[93] Flowers, G. E, Marshall, S. J, Björnsson, H, & Clarke, G. K. C. (2005) Sensitivity of vatnajökull ice cap hydrology and dynamics to climate warming over the next two centuries. *J. Geophys. Res.* **110 (F02011)**, doi:10.1029/2004JF000200.

[94] Ritz, C, Fabre, A, & Letréguilly, A. (197) Sensitivity of a greenland ice sheet model to ice flow and ablation parameters: consequences for the evolution through the last glacial cycle. *Clim. Dyn.* **13**, 11–24.

[95] Kamb, B & Echelmeyer, K. A. (1986) Stress-gradient coupling in glacier flow: I. longitudinal averaging of the influence of ice thickness and surface slope. *J. Glaciol.* **32**, 267–279.

[96] Marshall, S. J & Clarke, G. K. C. (1997) A continuum mixture model of ice stream thermomechanics in the laurentide ice sheet, 2. application to the hudson strait ice stream. *J. Geophys. Res.* **102 (B9)**, 20,615–20,638.

[97] MacAyeal, D. R, Bindschadler, R. A, & Scambos, T. A. (1995) Basal friction of ice stream e, west antarctica. *J. Glaciol.* **41**, 247–262.

[98] Vieli, A & Payne, A. J. (2003) Application of control methods for modelling the flow of pine island glacier, west antarctica. *Ann. Glaciol.* **36**, 197–203.

[99] Flowers, G. E & Clarke, G. K. C. (2002) A multicomponent coupled model of glacier hydrology, 1, theory and synthetic example. *J. Geophys. Res.* **107 (B11)**, doi:10.1029/2001JB001122.

[100] Johnson, J & Fastook, J. L. (2002) Northern hemisphere glaciation and its sensitivity to basal melt water. *Quaternary International* **95-96**, 65–74.

[101] Arnold, N. S & Sharp, M. J. (2002) Flow variability in the scandinavian ice sheet: modelling the coupling between ice sheet flow and hydrology. *Quat. Sci. Rev.* **21**, 485–502.

[102] Conway, H, Hall, B. L, Denton, G. H, Gades, A. M, & Waddington, E. D. (1999) Past and future grounding-line retreat of the west antarctic ice sheet. *Science* **286**, 280–283.

[103] Paul, F & Kotlarski, S. (2010) Forcing a distributed glacier mass balance model with the regional climate model remo. part ii: Downscaling strategy and results for two swiss glaciers. *J. Climate* **23 (6)**, 1607–1620.

[104] Toniazzo T, Gregory JM, H. (2004) Climate impact of a greenland deglaciation and its possible irreversibility. *J. Climate* **17**, 21–33.

[105] Ridley, J. K, Gregory, J, Huybrechts, P, & Lowe, J. (2010) Thresholds for irreversible decline of the greenland ice sheet. *Clim. Dyn.*

[106] Vizcaíno, M, Mikolajewicz, U, Gröger, M, Maier-Reimer, E, Schurgers, G, & Winguth, A. M. E. (2008) Long-term ice sheet-climate interactions under anthropogenic greenhouse forcing simulated with a complex earth system model. *Clim. Dyn.* **31**, 665–690.

[107] Holland, D. M, , Thomas, R. H, Young, B. D, Ribergaard, M. H, , & Lyberth, B. (2008) Acceleration of jakobshavn isbrætriggered by warm subsurface ocean waters. *Nat. Geosci.* **1**, 659–664.

[108] Walsh, J. E, Hibler III, W. D, & Ross, B. (1985) Numerical simultion of northern hemisphere sea ice variability 1951-1980. *J. Geophys. Res.* **90**, 4847–4865.

[109] Hibler, W. D. (1979) A dynamic thermodynamic sea ice model. *J. Phys. Oceanogr.* **9**, 815–846.

[110] Lipscomb, W. H, Hunke, E. C, Maslowski, W, & Jakacki, J. (2007) Improving ridging schemes for high-resolution sea ice models. *J. Geophys. Res.* **112:C03S91**, doi:10.1029/2005JC003355.

[111] Rothrock, D. A. (1975) The energetics of the plastic deformation of pack ice by ridging. *J. Geophys. Res.* **80**, 4514–4519.

[112] Hopkins, M. A & Hibler III, W. D. (1991) On the ridging of a thin sheet of lead ice. *Annals of Glaciology* **15**, 81–86.

[113] Flato, G. M & Hibler III, W. D. (1995) Ridging and strength in modelling the thickness distribution of Arctic sea ice. *J. Geophys. Res.* **C9**, 18,611–18,626.

[114] Dennis, J. M & Tufo, H. M. (2008) Scaling climate simulation applications on the ibm blue gene/l system. *IBM Journal of Research and Development: Applications for Massively Parallel Systems* **52(1/2)**, 117–126.

[115] Box, J. E, Bromwich, D, Veenhuis, B. A, Bai, L.-S, Stroeve, J. C, Rogers, J. C, Steffen, K, Haran, T, & Wang, S.-H. (2006) Greenland ice sheet surface mass balance variability (1988-2004) from calibrated polar mm5 output. *J. Climate* **19 (12)**, 2783–2800.

[116] Fettweis, X, Hanna, E, Gallée, H, Huybrechts, P, & Erpicum, M. (2008) Estimation of the greenland ice sheet surface mass balance for the 20th and 21st centuries. *The Cryosphere* **2**, 117–129.

[117] Wake, L. M, Huybrechts, P, Box, J. E, Hanna, E, Janssens, I, & Milne, G. A. (2009) Surface mass-balance changes of the greenland ice sheet since 1866. *Ann. Glaciol.* **50**, 178–184.

[118] Hopkins, M. A. (1996) On the mesoscale interaction of lead ice and floes. *J. Geophys. Res.* **101**, 18315–26.

[119] Kwok, R. (2001) in *IUTAM Scaling Laws in Ice Mechanics and Ice Dynamics*, eds. Dempsey, J, Shen, H, & Shapiro, L. (Kluwer Academic, 315–322).

[120] Hutchings, J, Heil, P, & Hibler, W. (2005) Modeling linear kinematic features in sea ice. *Mon. Wea. Rev.* **133**, 3481–3497.

[121] Hibler, W. D & Schulson, M. (2000) On modeling the anisotropic failure and flow of flawed sea ice. *J. Geophys. Res.* **105**, 17,105–17,120.

[122] Schreyer, H, Sulsky, D, Munday, L, Coon, M, & Kwok, R. (2006) Elastic-decohesive constitutive model for sea ice. *J. Geophys. Res.* **111:C11S26**, doi:10.1029/2005JC003344.

[123] Coon, M, Kwok, R, Levy, G, Prius, M, Schreyer, H, & Sulsky, D. (2007) Arctic ice Dynamcis Joint Experiment (AIDJEX) assumptions revisted and found inadequate. *J. Geophys. Res.* **112:C11S90**, doi:10.1029/2005JC003393.

[124] Arrigo, K. R, Kremer, J. N, & Sullivan, C. W. (1993) A simulated antarctic fast ice ecosystem. *J. Geophys. Res.* **98**, 6929–6946.

[125] Arrigo, K. R, Worthen, D. L, Lizotte, M. P, Dixon, P, & Dieckmann, G. (1997) Primary production in antarctic sea ice. *Science* **276**, 394–397.

[126] Lavoie, D, Denman, K, & Michel, C. (2005) Modeling ice algal growth and decline in a seasonally ice-covered region of the Arctic (Resolute Passage, Canadian Archipelago). *J. Geophys. Res.* **110**, C11009, doi:10.1029/2005JC002922.

[127] Jin, M, Deal, C. J, Wang, J, Tanaka, N, & Ikeda, M. (2007) Vertical mixing effect on the phytoplankton bloom in the southeastern bering sea midshelf. *J. Geophys. Res.* **111**, C03002. doi.10.1029/2005JC002994.

[128] Vancoppenolle, M, Goosse, H, de Montety, A, Fichefet, T, Tremblay, B, & Tison, J.-L. (2010) Modelling brine and nutrient dynamics in Antarctic sea ice: The case of dissolved silica. *J. Geophys. Res.* **115 C02005**, doi:/10.1029.2009JC005369.

[129] Bitz, C. M, Ridley, J. K, Holland, M. M, & Cattle, H. (2010) *Global Climate Models and 20th and 21st Century Arctic Climate Change. In Arctic Climate Change — The ACSYS Decade and Beyond*, ed. Lemke, P. (Springer), p. in press.